European Polymer Journal 183 (2023) 111762

Contents lists available at ScienceDirect

European Polymer Journal

journal homepage: www.elsevier.com/locate/europolj

Application of multipolymers system in the development of hydrogel-forming microneedle integrated with polyethylene glycol reservoir for transdermal delivery of albendazole

Ulfah Mahfufah [a], Nurul Aisha Fitri Sultan [a], Andi Maqhfirah Nurul Fitri [a], Diany Elim [a], Muhammad Alif Sya'ban Mahfud [a], Nurfadilla Wafiah [a], Rissa Ardita Friandini [a], Lutfi Chabib [b], Aliyah [a], Andi Dian Permana [a,*]

[a] Faculty of Pharmacy, Hasanuddin University, Makassar 90245, Indonesia
[b] Department of Pharmacy, Universitas Islam Indonesia, Yogyakarta 55584, Indonesia

ARTICLE INFO

Keywords:
Cystic echinococcosis
Hydrogel-forming microneedles
PEG reservoir
Albendazole

ABSTRACT

Parasitic infection is one of the health problems that cause many deaths in developing countries. One of the infectious parasites that is a problem for the world community is cystic echinococcosis (CE). The most popular medication for treating CE is albendazole (ABZ), however, it has limited intestinal absorption and poor water solubility, making it less effective. Therefore, developing an alternative ABZ delivery system is necessary to increase drug bioavailability and avoid first-pass metabolism. Here, we developed hydrogel-forming microneedles (HFM) combined with a polyethylene glycol (PEG) reservoir to deliver ABZ transdermally. HFM was made through a crosslinking process between polyvinyl alcohol (PVA) and polyvinyl pyrrolidone (PVP) as polymers and citric acid as a crosslinking agent. This HFM was developed to be integrated with a reservoir of polyethylene glycol (PEG) of varying molecular weights. HFM was successfully developed with desirable mechanical resistance and insertion properties. The evaluation of swelling capability resulted in >500 % swelling percentage. Moreover, the penetration result showed HFM could penetrate up to 68 % into the skin with only 3,83 % of height decrease. The skin integrity study also showed that the permeation of HFM into the skin caused no changes to skin integrity. Incorporated with a PEG reservoir, the *ex vivo* permeation test showed that 4584.43 ± 26.61 μg/cm^2 of ABZ was permeated through the skin. ABZ has been successfully developed into an HFM integrated with a PEG reservoir that is safe, painless, and non-irritating and has promising results for increasing the effectiveness of *cystic echinococcosis* therapy through the transdermal route.

1. Introduction

Parasitic infection is one of the health problems that cause many deaths in developing countries and even causes serious diseases in developed countries. One of the infectious parasites that is a problem for the world community is cystic echinococcosis (CE), caused by *Echinococcus* sp. The parasite enters the systemic circulation after infection and is accumulates in the liver and other organs, forming hydatidiform cysts [1]. CE has been considered a neglected tropical disease, whereas the World Health Organization (WHO) estimates that 1–3 million cases of disability have been reported each year as a result of this disease. This infectious disease is a major public health concern throughout the world, including areas of Asia, central South America, and even Mediterranean countries [2]. In Southeast Asia, a total of 49 cases of echinococcosis were identified from 1885 to 2015 [3]. Although not many cases have been reported, hepatic and pulmonary echinococcosis complications can be a major cause of death (see Fig. 1).

There are currently several options for the treatment of CE, including antiparasitic administration, percutaneous drainage therapy, and surgical intervention. In many inoperable conditions, such as brain cysts, antiparasitic administration is the first and only option [4]. Albendazole (ABZ) is the most effective drug commonly used to treat CE at present [5]. However, ABZ has poor intestinal absorption and water solubility. ABZ taken orally has a bioavailability value of<5 % and is erratic, making it less effective [6]. Oral administration of ABZ also causes first-pass metabolism in the liver [7]. This causes a lack of effectiveness and

* Corresponding author.
E-mail address: andi.dian.permana@farmasi.unhas.ac.id (A.D. Permana).

https://doi.org/10.1016/j.eurpolymj.2022.111762
Received 6 October 2022; Received in revised form 6 December 2022; Accepted 7 December 2022
Available online 12 December 2022

results in the drug having to be taken in high doses. This can cause side effects such as liver toxicity and gastrointestinal toxicity. Therefore, to overcome low solubility and increase the effectiveness, an alternative delivery system must be developed.

One of the delivery systems that can avoid ABZ metabolism in the liver and increase the effectiveness of ABZ in medicine is the microneedle (MN) delivery system. MNs are minimally-invasive arrays consisting of numerous micron-sized needles assembled on a baseplate [27], which can penetrate through the stratum corneum and enable drug penetration without reaching the nerve and blood vessels and, thus, are minimally invasive [8]. These formulations can easily be used to deliver drugs into the deeper of skin layer, through absorption of interstitial fluid and thus be swollen, allowing the drug to diffuse from the reservoir down its concentration gradient towards the hydrogel matrix and then into the skin layer, where it finally reaches the systemic circulation [9].

Hydrogel forming microneedle (HFM) is a type of microneedle (MN) that is made by crosslinking an aqueous polymer mixture. This type of MN consists of a micron-scale needle arranged on a base plate and contains no drug but is contained in a reservoir attached to the base plate's upper side. MN with the hydrogel-forming model would swell if it absorbs interstitial skin fluid. HFM initially acts as a tool to penetrate the barrier *stratum corneum*. After insertion, the hydrogel would act as a membrane rate control of drug entry into the systemic circulation [10]. Several previous studies have shown that repeated application of MNs into the skin does not cause a decrease in skin barrier function. In addition, the use of polymer-based MNs, such as HFMN, has been shown not to stimulate the humoral immune system. The hydrogel-forming MN delivery system, which swells when it absorbs skin interstitial fluid, and stimulates drug permeation from the attached reservoir, makes this HFMN array biocompatible with good characterization [11].

In the HFM system, it is necessary to consider reservoir, which is used as a drug holder attached to the top side of the MN. Reservoir polyethylene glycol (PEG) integrated with HFM can provide faster drug action and less drug delivery limited [12]. PEG is a hydrophilic carrier that can increase drug solubility with low toxicity when compared to other polymers. PEG was found to be a suitable reservoir medium for enhancing the transdermal delivery of hydrophobic compounds [13]. This form can be integrated quickly for the release, dissolved and dispersed drugs. Through this reservoir shape, the onset time of ABZ reservoir can be increased with PEG so that it has the potential to increase its bioavailability [14].

Some of the ingredients that have been often used in making hydrogels are a combination of polyvinyl alcohol (PVA) and polyvinyl pyrrolidone (PVP), using citric acid as a crosslinking agent because these materials are safe and biocompatible [15]. In the body, PVA can be decomposed through a hydrolysis mechanism so that it is widely used in biomedical fabrication, as in making microneedles. The presence of recurring hydroxyl groups in the PVA structure makes it ideal for physical and chemical cross bonds so that it is widely used to form a polymer base [16]. Moreover, the addition of PVP to PVA polymer can produce good microneedle mechanical properties [17].

This study is the first to formulate ABZ via a transdermal route in the HFM integrated with the PEG reservoir. This study aimed develop and investigate the difference in HFM heating time to determine the optimal time in the ABZ formulation into an integrated HFM PEG reservoir through characterization parameters and profile of the amount of drug permeation parameters. In addition, the proper formulation of drug reservoirs was also being explored. The resulting system was further characterized by evaluating the physical characteristics of the HFM integrated PEG reservoir and drug delivery capacity through ex vivo permeation studies as a determinant of the most optimal formula.

2. Materials and methods

2.1. Materials

Albendazole (ABZ) (purity, 98 %) of analytical grade was obtained by Alfa Aesar (Lancashire, U.K). Polyvinyl alcohol (PVA) was purchased from Sigma-Aldrich Pte Ltd. (Singapore, Singapore), and polyvinyl pyrrolidone (PVP) K30 was purchased from Fadjar Kimia (Bogor, Indonesia). Citric acid and polyethylene glycol (PEG) 6000 were purchased from Merck Schuchardt OHG (Hohenbrunn, Germany). PEG 400 and Tween80® were purchased from idCHEM Co., Ltd. (Gyeonggi, South Korea). Phosphate-buffered saline (PBS) tablet was purchased from Dulbecco A Oxoid® Ltd. (Hampshire, United Kingdom). Distilled water was purchased from PT Jayamas Medica Industri (Sidoarjo,

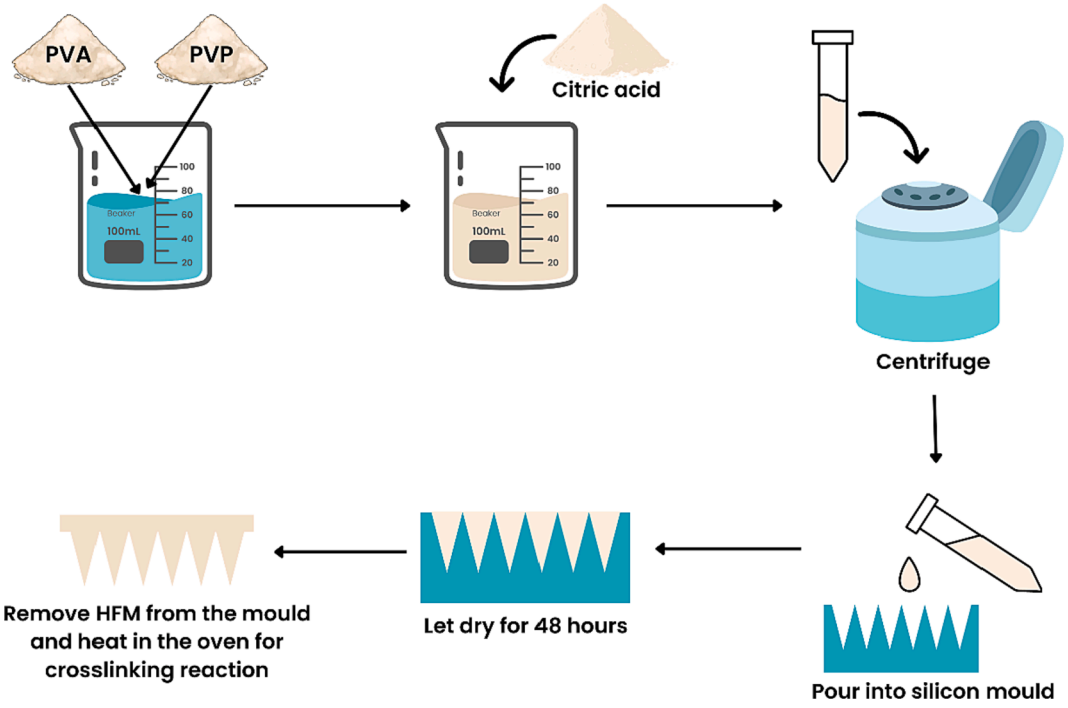

Fig. 1. Schematic illustration of the HFM's preparation.

Indonesia). Other chemicals and materials were all of analytical grade.

2.2. Saturation solubility study

This study was carried out to assess the solubility of ABZ in various solvents. The saturated solubility of ABZ was measured by placing 1 mL of various solvents and solvent mixtures consisting of PEG 400, Tween80, and PBS at various pH in each vial. Then ABZ is added to each vial and homogenized using Vortex® mixer until the solution becomes cloudy. All vials were shaken in an orbital shaker (Optima® OS-752, Japan) at100 rpm at a temperature of ± 37 °C for 24 h. Then it was centrifuged to separate the remaining residue. The supernatant was collected and filtered through a 0.20 μm syringe filter and measured using a UV–Vis spectrophotometer [11].

2.3. Preparation of hydrogel

Hydrogel film formulations contain PVA and PVP as polymers and citric acid as the crosslinking agent. Initially, PVA and PVP were dissolved in water until homogeneous. Then, citric acid was added and stirred until homogeneous. The mixture was centrifuged (LC-04S Centrifuge, Zenith Lab (Jiangsu) Co., LTD.) at 3500 rpm for 15 min [16]. The formula was then poured into a petri dish and dried at room temperature for 48 h. After drying, the film was crosslinked at 130℃ [18] for the time shown in Table 1 for each formula.

2.4. Swelling study and gel fraction analysis

The swelling study was carried out by weighing the hydrogel film in a dry state and the initial weight recorded, then immersed in a PBS solution of pH 7.4 and reweighed at time intervals of 0.25, 0.5, 1, 2, 3, 4, 5, 6, 8, and 24 h. To remove excess PBS from the film's surface, it was dried with filter paper. The percentage of swelling is then calculated using **Equation (1)**, where m_1 is the weight of the 24 h swollen hydrogel and m_0 is the initial weight of the hydrogel [16,17]:

$$\%\,\text{Swelling} = \frac{(m_1 - m_0)}{m_0} \times 100\% \quad (1)$$

The gel fraction analysis was carried out to determine the elasticity of the hydrogel, which indicates the percentage of gel fraction (%GF). The fully hydrated segments of hydrogel membrane that had been soaked for 24 h in the swelling test was dried at 50 °C for 24 h, then the hydrogel membrane was weighed (m_d). The result of gel fraction (GF%) was determined by calculating the weight ratio between dehydrated hydrogel membrane weight (m_d) with the initial weight of the hydrogek (m_0) by **Equation (2)** [20].

$$\%\,\text{GF} = \frac{m_d}{m_0} \times 100\% \quad (2)$$

2.5. Scanning electron microscope (SEM)

The morphology of the hydrogel film was evaluated by using scanning electron microscopy (SEM). Surface morphology of hydrogel film from each formula was studied using Quanta FEG 250 benchtop scanning electron microscope (SEM) (FEI, Hillsboro, OR, USA) at an acceleration voltage of 15 kV.

Table 1
Hydrogel film formulation at various crosslinking temperatures.

Formula	Composition in water (%w/w)	Crosslinking Time (minute)
F1	15 % PVA, 10 % PVP, 1.5 % CA	40
F2	15 % PVA, 10 % PVP, 1.5 % CA	80
F3	15 % PVA, 10 % PVP, 1.5 % CA	120

2.6. Fabrication of hydrogel-forming microneedle (HFM)

The manufacture of HFM was carried out using the formula in Table 1. Initially, 0.5 g aliquot of each aqueous polymeric blend was poured into the MN silicone moulds (needle density 10 × 10, conical shape, 700 μm height), then centrifuged at 3500 rpm for 30 min. The HFM arrays were dried at 37 °C for 48 h [16]. After drying, HFM were removed from the moulds and heated at 130 °C with the time as shown in Table 1 for each formula.

2.7. Mechanical resistance and insertion properties of HFM

This study was carried out to hepatic and pulmonary echinococcosis complications measure the percentage reduction in needle height after being given a force equivalent to manual compression force. A microneedle was applied, and a pressure equivalent to 32 N/array was applied for 30 s. The percentage of mechanical resistance and penetration ability is calculated using **Equation (3),** where H_0 is needle height before compression and H_c is needle height after compression [21].

$$\text{Height reduction}\,(\%) = \frac{H_0 - H_c}{H_0}\,\text{x}\,100\% \quad (3)$$

Insertion properties were determined by the number of holes created in each layer of the Parafilm M® and observed using a light microscope. The deepest layer of the hole was specified [18].

2.8. Surface pH

Surface pH was assessed by immersing 20 mg of HFM in 50 mL of double distilled water and allowing it to stand at room temperature for 15 min. Next, the composite electrode was placed on the surface of the HFM and the pH was measured after equilibration for 1 min [22].

2.9. Water vapour transmission

WVT was evaluated by filling anhydrous calcium chloride into glass vials and sealing it with hydrogel film and tape. The vials were then stored in a desiccator containing saturated potassium chloride solution for 14 days [22]. WVT was calculated using **Equation (4)**, where V_t was the vial's final weight, and V_0 was the vial's initial weight [23].

$$\text{WVT} = \frac{(V_t - V_0)\,\text{x film thickness}}{\text{film surface area}} \quad (4)$$

2.10. Moisture absorption ability (MAA)

The ability of hydrogel film to absorb moisture from various conditions was examined in an MAA investigation previously described [24], with minor modification. Initially, three desiccators with various types of relative humidity (RH) were used to keep hydrogel film. The hydrogel film was stored in three different desiccators, which contain magnesium chloride (33 % RH), sodium nitrite (65 % RH), and potassium sulfate (97 % RH). The film made of hydrogel was kept for 14 days while being weighed every 24 h. The study's findings are based on the MAA percentage obtained from **Equation (5)**.

$$\%\text{MAA} = \frac{\text{Mass of HFM in desiccator} - \text{Initial mass of hydrogel film}}{\text{Initial mass of HFM}} \quad (5)$$

2.11. Preparation of PEG (polyethylene glycol) reservoirs

Albendazole-PEG solid dispersion reservoir tablets were prepared according to the composition listed in Table 2. Initially, a mixture of PEG was heated using an oven at 70 °C for 15 min. The PEG mixture was removed from the oven, and the ABZ was added while mixing vigorously until homogeneous then, the reservoir mixture was put back into the

Table 2
Composition of PEG reservoir's formula.

Composition (%w/w)	R1	R2	R3
Reservoir's Composition			
Albendazole	20	20	20
PEG mixture	80	80	80
PEG Mixture Composition			
PEG 400	25	50	75
PEG 6000	75	50	25

oven for 15 min. The reservoir was formed by pouring 250 mg of the mixture into a silicone mould and cooling at 4℃ for 15 min.

The PEG reservoir was made using the modified solid dispersion method [18] with the compositions listed in Table 2. PEG 400 was used as a liquid cosolvent, and PEG 6000 as solid base. First, a mixture of drug and PEG was made by dispersing ABZ in PEG 400 and mixing vigorously until homogeneous. The weighed PEG 6000 was added to the mixture and put into the oven at 70℃ for 30 min. The reservoir was formed by pouring 250 mg of the mixture into a silicone mould with a size of 100 mm × 100 mm. Lastly, the reservoir was refrigerated at 4 °C for 15 min to make the reservoir solid.

2.12. Characterization of PEG reservoirs

2.12.1. Physical properties of PEG reservoirs

This study was carried out by measuring the hardness and dissolution time. The reservoir was placed in the hardness tester instrument (Sotax® HT1, India), and its diameter was measured. After that, the tool applied pressure to the reservoir until the sample was damaged. Meanwhile, the dissolution time was measured by immersing the PEG reservoirs at 20 mL PBS pH 7.4, stirring at 6000 rpm, and specifying the time until the entire reservoirs were dissolved [18].

2.12.2. X-ray diffraction (XRD)

XRD study was carried out using pure albendazole and its mixtures with various reservoirs. All samples were measured using an X-ray diffractometer instrument (Rigaku®, Japan) using CuKa radiation at 40 kV and 30 mA. All the data were recorded over 2θ range of 10 – 80°, with a scanning speed of 4°/min and at a preset time of 0.2 s [25].

2.12.3. Differential scanning Calorimetry (DSC)

Differential Scanning Calorimetry (DSC) thermograms analysis was carried out to investigate the physical condition of ABZ in the PEG reservoir formulation. Thermograms of pure ABZ, reservoir 1 (R1), reservoir 2 (R2), and reservoir 3 (R3) was recorded using the DSC model Q20 V24.2 Build 107 (Universal V4.5A TA Instruments). The samples were heated using a standard aluminium pan at a temperature of 0–300 °C at a heating rate of 5 °C/min [22,23].

2.13. Fourier transform infrared spectroscopy (FTIR)

FTIR study was carried out using pure albendazole and its mixtures with various reservoirs. The sample was analyzed in an FTIR spectrophotometer (Shimadzu® IR Prestige-21, Japan) under identical conditions using the potassium bromide pellet method with the scanning region of 4000 – 400 cm^{-1} at 2 cm^{-1} resolution [25].

2.14. Ex vivo permeation study

This study was carried out using rat skin membranes placed in the donor compartment of Franz diffusion cells, with the *stratum corneum* facing the donor compartment [22]. MN was applied to the skin of the rat and pressed with the help of a disposable syringe plunger for 30 s. A 5 g load was placed on top of the MN, then the donor compartment was closed using Parafilm M® and mounted on the receptor compartment. The medium used in the receptor compartment was PBS solution (pH 7.4) at 37 ± 10 °C and stirred at 100 rpm. Sampling from the receptor compartment was carried out simultaneously at intervals of 0.5, 1, 2, 3, 4, 5, 6, 7, 8, and 24 h. The results of the samples were then analyzed using spectrophotometry at the maximum wavelength of ABZ.

2.15. Skin integrity

FTIR was utilized to evaluate the integrity of skin structure in order to ascertain how the administration of HFM will affect the skin structure [19,24]. Following the *ex vivo* permeation investigation, rat skin samples that had been taken out of the compartment were cleaned and subjected to an FTIR analysis. Investigations were also conducted to compare treated skin to untreated skin used as a control.

2.16. Hemolytic test

Rat red blood cells were utilized in an initial toxicity test for the created preparation known as a hemolytic assay. The approach used is in line with previous research, with a slight variation [4,19,25]. Blood was first centrifuged for 20 min at 2000 rpm. Following that, plasma was withdrawn, and red blood cells were cleaned three times with PBS to produce a clear supernatant. The centrifuged red blood cells were then combined with PBS to a final concentration of 10% v/v. The test sample was prepared in three concentration levels of 500, 50, and 5 ppm and diluted using PBS. 100 μL of red blood cell suspension were added for every 900 μL of the sample, and the mixture was incubated at 37 °C for 60 min. Additionally, an aquadest positive control and a PBS negative control were created. The mixture was then centrifuged at 7000 rpm for 10 min after incubation, and the supernatant was taken and analyzed at 540 nm using a UV–Vis spectrophotometer. **Equation (6)** was used to determine each formula's hemolytic percentage.

$$\%\text{Hemolytic} = \frac{\text{Sample absorbance} - \text{Negative control absorbance}}{\text{Positive control absorbance} - \text{Negative control absorbance}} \times 100\% \quad (6)$$

2.17. Statistical analysis

All experimental data were provided as means and standard deviation (SD). GraphPad Prism® version 8.0 was used for statistical analysis (GraphPad Software, San Diego, California, USA). The analysis of variance (ANOVA) in One-Way was carried out to compare different groups. Statistical significance was always indicated by using a value of $p < 0.05$.

3. Results and discussion

3.1. Saturation solubility study

ABZ belongs to the BCS class II category, with good permeability and poor solubility [6]. This study was carried out to compare the solubility of ABZ in various solvents and a combination of solvents that could potentially improve the solubility of ABZ. In addition, this assay is performed to determine the best combination of solvents that can be used as a dissolution medium [28]. The results obtained can be seen in Table 3, where the highest solubility of ABZ was received from a combination of PBS pH 7.4 with Tween80 2 % (283.62 ± 11.39 μg/mL), and the lowest solubility was obtained from a combination of PBS pH 7.4 with Tween80 1 % (135.62 ± 11.43 μg/mL). Compared to solubility in PBS pH 7.4, solubility in PBS pH 7.4 with Tween80 2 % was increased up to 5-fold. Surfactant, like Tween80, could increase solubility by reducing the surface tension of the solid drug, increasing the drug's wetting to a higher degree [28–31]. Therefore, a combination of PBS pH 7,4 with Tween80 2 % was selected as the preferred solvent combination

Table 3
Saturated solubility of albendazole in various solvents (n = 3).

Solvent	Solubility (μg/ml)
PBS pH 7,4 + PEG400 10 %	138.14 ± 0.91
PBS pH 7,4 + PEG400 20 %	146.90 ± 1.03
PBS pH 7,4 + Tween80 1 %	135.62 ± 11.43
PBS pH 7,4 + Tween80 2 %	283.62 ± 11.39
PBS pH 7,4	48.11 ± 1.82
PBS pH 6,8	47.77 ± 1.91
PBS pH 5	38.14 ± 1.57

due to its proven effectiveness in enhancing the solubility of ABZ (see Table 4).

3.2. Preparation of hydrogel and swelling studies

MN is a delivery system with transdermal penetration of drugs consisting of a collection of micro-sized needles capable of delivering drugs directly into the systemic circulation [9]. HFMs are one type of MN that are made through a crosslinking process from polymer and crosslinking agent mixture. It consists of a micron-scale needle arranged on a base plate with the drug stored in a reservoir attached to the upper side of the base plate. Once inserted into the skin, it absorbs interstitial fluid from the underlying skin tissue and allows the drug diffuse from the reservoir to the skin microcirculation and eventually reach the systemic circulation. HFM delivers various molecules effectively, such as hydrophilic, hydrophobic, high-molecular, and high-dose substances. HFM has the advantage of being able to be removed from the skin so that it will not result in polymer deposition in the skin, and the drug delivery is not limited to the needle contained only [18].

The swelling test was carried out to determine the swelling ability of MN when it was inserted into the skin. Hydrogel forming will expand when inserted into the skin because it absorbs interstitial fluid. Fig. 2**A** shows that the formulas with a swelling percentage from the highest to the lowest. F1, F2, and F3 showed the value of the swelling percentage of 509.27 ± 1.99 %; 418.80 ± 2.50 %; and 400.21 ± 5.85, respectively. This indicates that the variation of the heating time used affects the swelling percentage of the hydrogel film. The longer the heating time, the lower the swelling percentage. Similarly, the results of statistical analysis showed that the percentage of swelling of F1 to F2 and F3 was significantly different ($p < 0.05$), but the percentage of swelling of F2 to F3 was not significantly different ($p > 0.05$).

Variations of crosslinking temperature affect the degree of crosslinking between PVA chains and citric acid [16]. This result was the same as previous studies, which was expected since increasing the heating time significantly decreases the swelling percentage [13,16]. The MN expands as it absorbs interstitial fluid when placed on the skin, leading to a channel between the reservoir and the systemic circulation [32]. When the heating time is increased, the formation of ester bonds between the polymer and citric acid will be higher, so that many crosslinks occur [18]. This has the effect of decreasing the swelling percentage of film because the liquid would be difficult to penetrate the film structure [33]. This phenomenon occurs because the increased evaporation of water facilitates the esterification reaction from the reaction system due to the increase in kinetic energy by high temperature [34].

3.3. Fabrication and characterization of HFM

The formation of hydrogen bonds between PVA, which has the –OH group, and PVP, which has the C═O group, has been demonstrated in earlier research to increase the mechanical strength of microneedles [35]. Additionally, citric acid as a crosslinking agent, strengthens the HFM matrix by binding to the –OH group through an esterification reaction [36]. Fig. 2**C and 2D** showed the morphology of HFM that was observed using a light microscope, revealing that the HFM formed a sharp needle tip. All HFM formulations produced a needle height of < 1500 μm, allowing the drug to be released across the epidermis into the deep dermis. Because the distance from the outermost layer of skin to the dermis has a thickness of up to 2000 μm [37], the use of this HFM formulation can penetrate the *stratum corneum* but cannot reach the nerve endings, so it causes no pain [32].

HFM is made through a cross-linking process so that no polymer will dissolve during insertion. However, if some uncrosslinked polymers happens to be depositted into the skin upon the HFM application, it can be assumed that the biodegradable properties would provide safety assurance. Previous study has assessed the use of PVA-made MNs which are injected daily into mice for 160 days, there was no evidence of toxicity found. It was discovered that the concentration of PVA decreased over time, indicating dissolution, diffusion, or degradation of PVA in the skin [38]. In addition, we have also done the hemolytic assay for the system initial toxicity screening which resulted in satisfactory result. With respect to the polymer used, PVA and PVP undergoes slow rate of biodegration. According to previous study on the elimination of macromolecules after administration to the skin, the majority of the polymers with molecular weights below 66 kDa are predicted to be drained into the dermal blood capillaries with only a small amount being drained into the dermal lymphatics before reaching the systemic circulation [39]. Polymers with a molecular weight of<60 kDa will be excreted by the renal as a result of glomerular filtration upon reaching the systemic circulation [38,40].

The mechanical strength test of HFM was carried out to determine the ability of the MN to penetrate the skin layer, namely the *stratum corneum* in order to deliver drugs properly [17]. Mechanical strength was evaluated to determine the microneedle's strength when given pressure of 30 N.

Fig. 2**C and 2D** show the difference between the needles before and after the mechanical resistance and insertion properties study. Each formula shows a curved needle after testing. This was probably due to the different mechanical strengths of each needle. The faster the heating time, the lower the mechanical strength so that the tested needle is more curved and can only penetrate a few layers of Parafilm M®. In this test, it can be seen that there was no damaged MN after being given mechanical strength but only bent. It showed good mechanical properties and was suitable for making strong HFM [16]. The mechanical strength of HFM was measured based on the percentage decrease in needle height before and after testing.

The average size of the MN is made with a length of 150–1500 μm, which corresponds to the needle's length that can penetrate the skin. This size corresponds to the thickness of the skin to the dermis but does not reach the nerve endings, so it cause no pain when applied [32]. Needles that have a size of>1500 μm can reach the bottom of the dermis which is located at the end of the nerve endings. Therefore, any microneedle formula made is painless.

Fig. 2**E** showed the percentage of the greatest decrease in needle height that was found in F1 of 17.76 ± 0.06 %, while the lowest reduction in needle height was in F3, which was 3.83 ± 0.19 %, so the formula that has the best mechanical strength is F3. This shows that the heating time used affects the strength and size of the MN. The faster the heating time, the greater the percentage reduction in MN height. Statistically, the values were significantly different ($p < 0.05$). This result indicates that these HFM formulas have adequate mechanical strength.

This is in accordance with a previous study, which stated that a faster crosslinking time could produce a softer needle so that it has lower mechanical resistance. Likewise, a longer crosslinking time can produce needles with a stronger structure due to the increased degree of

Table 4
Ex vivo permeation parameters of HFM combined with reservoir R3.

Permeation Parameters	F1	F2	F3
Flux at 24 h (μg/cm^2.h)	191.02	162.96	153.61

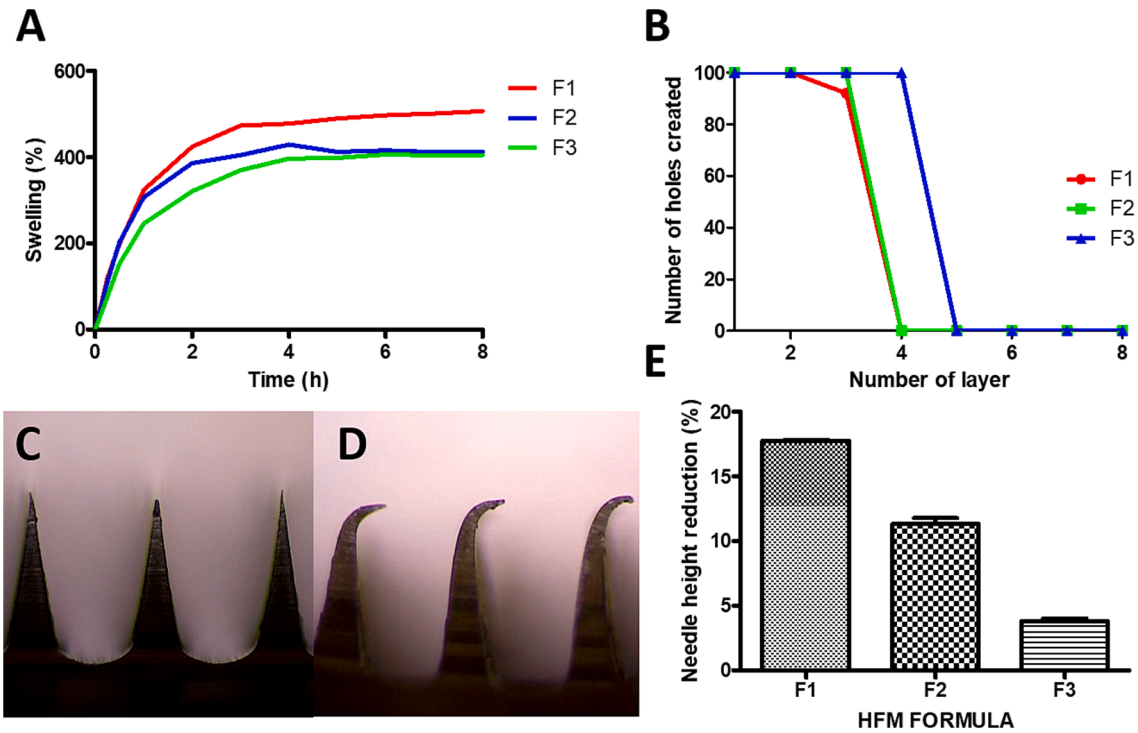

Fig. 2. Swelling behaviour of hydrogel film with different crosslink temperatures (A); penetration ability of HFM on each crosslink temperature; representative microscopic view of HFM (4x magnification) before (C) and after (D) compressed when applied through Parafilm M®; comparison of mechanical strength of HFM prepared (means + SD, n = 3) (E).

crosslinking so that they have higher mechanical strength [41]. If the microneedle structure is too rigid, the HFM may fracture upon insertion into the skin leaving an insoluble polymer, which is highly undesirable [16].

The penetration ability of MN is a study conducted to confirm the results of the mechanical resistance evaluation and determine MN's penetrating power based on observations of the holes formed in each layer of parafilm M®. Each layer of parafilm M® has an average thickness of 126 μ m, and for 8 layers of parafilm M®, it has a thickness of 1008 μm or equivalent to the thickness of the skin *corneum* layer to the upper dermis [17].

Insertion properties were evaluated in order to make sure that HFM can penetrate the artificial skin test model to deliver the drug into the *stratum corneum.* As presented in Fig. 2**B**, it is found that F1 and F2 can penetrate parafilm M® to form a third layer with 92 holes (92 %) and 100 holes (100 %), respectively. The F3 can penetrate up to the fourth layer by forming 100 holes (100 %) which was equivalent to 504 μm (Parafilm M® layer thickness = 126 μm) or 68 % of the microneedle height. This is in accordance with the mechanical resistance test which showed that F3 had the greatest mechanical strength among the other two MN formulas, so that only F3 was able to penetrate up to the fourth layer. The MN penetration obtained by each formula was not significantly different ($p > 0.05$) and showed the HFM formula was long enough to penetrate the skin to the dermis.

HFM innovation tends to increase patient acceptance and convenience due to its ease of application. This device can be applied by hand, to allow ease of use by the patients. Previous studies reported that microneedles could be applied using the thumb for 30 s with a pressure of 32 N per array, like the patients pushing an elevator button or pressing a stamp onto an envelope [42]. A pressure-indicating sensor can be used to ensure that the pressure given is appropriate. The pressure-indicating sensor will change its colour when the applied forces reach 30 N and even be more concentrated if given a greater force [43]. The use of a method of feedback to ensure reproducible insertion is preferable to an applicator, assisted by a patient information leaflet and pharmacist counselling [44].

3.4. Surface pH

The surface pH was evaluated to ensure skin tolerance when the hydrogel was applied. This assay is important because an unsuitable pH potentially irritates the skin. As presented in Fig. 3**A**, the surface pH values of F1, F2, and F3 are 5.48 ± 0.41, 5.51 ± 0.34, and 5.43 ± 0.43, respectively, and these values were not significantly different ($p > 0.05$). In addition, the results show a pH value close to the skin's normal pH, which is 5.8 (3), so it can be concluded that HFM is non-irritating and non-invasive [22].

3.5. Water vapour transmission

Evaluation of water vapour transmission (WVT) was carried out to determine the stability of the hydrogel in high-humidity environmental conditions. The results of WVT are shown in Fig. 3**B**, the transmission rates obtained were 0.59 ± 0.15, 0.54 ± 0.16, 0.56 ± 0.09 μg.cm/cm^2 for F1, F2, and F3, respectively. This result shows a lower value than the previous study [45] and indicates the long-term stability of the hydrogel due to less water loss capability [22]. In addition, statistically, these results showed no significant difference ($p > 0.05$).

3.6. Moisture absorption ability

This study has been performed to examine the absorption ability of HFMs through different environmental conditions. The HFMs were stored in three different desiccators, which contain magnesium chloride (33 % RH), sodium nitrite (65 % RH), and potassium sulfate (97 % RH). The increased water absorption ability is followed by an increased RH value which is shown in Fig. 3**D-3F**. After treatment for 14 days, the total %RH for the whole formula was < 10 %. The formula finds the lowest percentage moisture absorption ability with the lowest crosslinking heat-treatment duration. The lowest heat-treatment duration can reduce

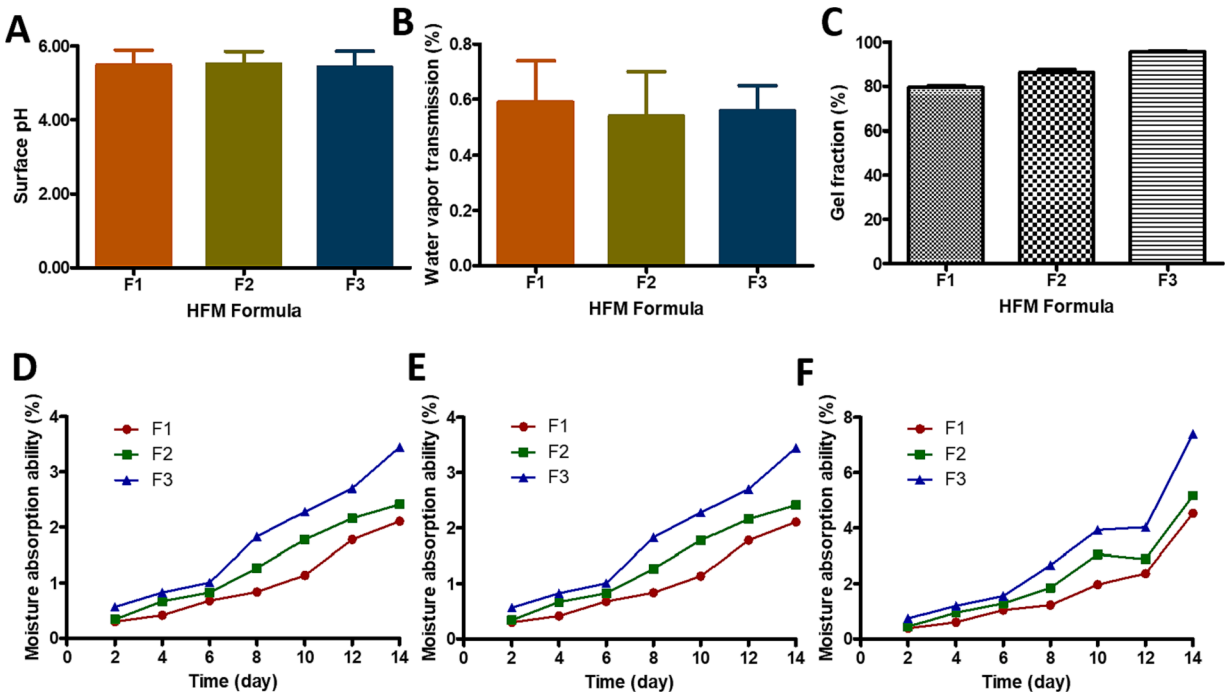

Fig. 3. Surface pH (A), water vapour transmission (B) (mean ± SD, n = 3), percentage of gel fraction of each formula (C) (mean ± SD, n = 3), also moisture absorption ability at RH 33 % (D), RH 65 % (E), and RH 97 % (F) for all HFM formulas.

the crosslinking ability, which can reduce the elasticity of the HFMs [18]. The low elasticity of HFMs can decrease the moisture absorption ability [46]. In addition, the PVP contained in HFMs also affects the ability to absorb moisture because it is a hydrophilic polymer that has interactions with water [47].

3.7. Gel fraction

In general, the gel fraction (GF) describes the flexibility of a hydrogel that is formed. Hydrogels with low flexibility can exhibit complex characteristics and difficulties in absorbing fluids, including interstitial fluids [16]. As shown in Fig. 3**C**, it is known that the GF (%) of F1 (79.42 ± 0.81 %), F2 (86.26 ± 1.25 %) and F3 (95.62 ± 0.44 %) and the highest %GF is obtained when HFF was crosslinked for 120 min. All formulas differed significantly in percentage of GF ($p < 0.05$). The results obtained showed that GF % decreased with increasing the duration of heating time. Furthermore, GF % provides more information about the effectiveness of the crosslinking process in forming the insoluble fraction. Based on the GF test, increasing the heating duration can potentially decrease the swelling capacity by limiting the PVA chains and reducing the water absorption capacity [48].

3.8. Scanning electron microscope (SEM)

SEM was used to examine the morphology of the HFFs to determine the effect of crosslinking time on their characteristics. Fig. 4 shows representative SEM images of crosslinked hydrogel film prepared from each formula. HFF crosslinked for 40 min (F1) showed a porous structure (Fig. 4**A**). However, HFF crosslinked for 80 min (F2) formed a more solid structure and 120 min (F3) showed a smooth surface with a decreasing pore size that could barely be detected by SEM. This may be due to the longer crosslinking time, which caused a significant increase in the crosslinking degree, resulting in more crosslinking points and HFF with much smaller pore sizes [19].

3.9. Preparation and physical properties of PEG reservoirs

The drug in the reservoir attached to the hydrogel plate forms an MN which, after entering the skin, will absorb interstitial fluid from the skin tissue, allowing the drug to diffuse from the reservoir layer to the skin microcirculation [18]. MN mechanism creates airways in the skin to facilitate the delivery of poorly soluble drugs, which are dispersed in a hydrophilic matrix [11]. PEG is a hydrophilic carrier that can increase drug solubility with low toxicity when compared to other polymers. PEG

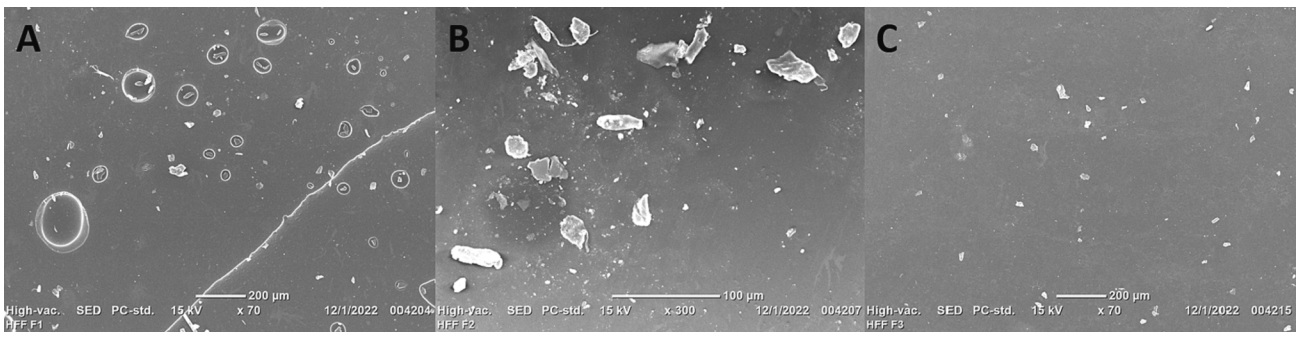

Fig. 4. SEM images of HFF prepared from (A) F1, (B) F2, and (C) F3.

is a suitable reservoir medium to increase the transdermal delivery of hydrophobic compounds [13]. The drug reservoir's hardness is essential because the drug reservoir has to accommodate the minimum liquid medium provided by the HFM [10]. As shown in Fig. 5**F**, the hardness of the reservoir found is 33 N/cm^2, 31.67 N/cm^2, 31 N/cm^2 for R1, R2, and R3, respectively. The results showed that an increase in the concentration of PEG 400 proportions caused a decrease in the mechanical strength of the reservoir. Still, these results showed no significant difference in each formula ($p > 0.05$). The R3 has the lowest hardness because it contains more PEG 400 than the other two formulas, which has the lowest molecular weight compared to PEG 6000, affecting the hardness. The greater the percentage of low molecular weight PEG, the softer the resulting reservoir [18].

The dissolution time study has a correlation with the rate of diffusion of the drug that has dissolved from the reservoir into the aqueous medium, which has become an important parameter that is continued in the ex vivo permeation test [49]. The dissolution time of R1 to R3 decreased significantly ($p < 0.05$) along with the increase in the concentration of PEG 400 as shown in Fig. 5**G**. The concentration of PEG 400, which is greater than PEG 6000 in R3 has the lowest molecular weight compared to other formulas. PEG 400 is a type of polymer with the lowest molecular weight, which can affect the duration of dissolution time. Polymers with low molecular weights have a faster dissolution time than polymers with large molecular weights [50]. Thus, the ratio of PEG concentrations significantly affects the dissolution time of the reservoir. Therefore, R3 is the optimal formula used in ex vivo permeation studies because it has a hardness value that meets the requirements and the shortest dissolution time compared to other formulas.

3.10. X-ray diffraction (XRD) and Differential scanning Calorimetry (DSC)

Analysis of XRD was performed to ensure the presence and change of crystalline properties of albendazole in PEG reservoirs, which indicated their solubility in the reservoirs [22,36]. Characteristic peaks of pure albendazole were found at diffraction angles 14.54, 16.84, 19.92, and 24.13, as presented in Fig. 5**D**. Compared to the XRD pattern of albendazole, R1 and R2 showed similar peaks with pure albendazole. Meanwhile, R3 showed a change in the peaks, the peaks' intensity was specifically decreased. The result suggests the change of crystallinity of albendazole in the reservoir matrix, which began to reach an amorphous form and increase in solubility [22,36].

DSC was carried out to investigate any physical change in the drug upon the fabrication process into the reservoir [51]. The DSC thermogram of pure ABZ, reservoir 1 (R1), reservoir 2 (R2), and reservoir 3 (R3) showed in Fig. 6**A**. An endothermic peak for pure ABZ, R1 and R2 was found at 195 °C and 209 °C. A sharp peak of pure ABZ appeared at 195 °C, showing collapse temperature indicates the melting point and a small peak at 209 °C indicates the recrystallization process. Both peaks on R1 and R2 are still detected so that ABZ is still in the form of crystals when formulated in the form of R1 and R2. R3 did not show peaks at 195 °C and 209 °C like the two previous reservoirs, indicating that the ABZ structure has changed to amorphous. The absence of those peaks in R3 showed the possibility that hydrogen bonding could reduce ABZ crystallinity and form an amorphous state. The amorphous form of ABZ was easier to dissolve and better delivered due to increased solubility [52]. It has been known that the transformation from a crystalline state of a drug to an amorphous state causes a high energy state and high disorder, thereby increasing the solubility and dissolution rate [53]. This is in accordance with the results of the reservoir dissolution test in **Section 3.9**. Hence, R3 is preferable due to its higher dissolution time, and it was chosen to proceed to the *ex vivo* permeation study.

3.11. Fourier transform infrared spectroscopy (FTIR)

Analysis using FTIR was designed to ensure the presence of ABZ in the formulated reservoir. Fig. 6**E** showed that ABZ exhibited wavenumber at 1193 cm^{-1} describes the C—O—C bond, 1635 and 1572 cm^{-1} describe N–H out of the plane bending of ABZ structure, 1709 cm^{-1} for carbonyl groups, 2935 and 2878 cm^{-1} for C–H stretching, 3331 cm^{-1} for N–H stretching, and lastly 2705 cm^{-1} that describe the hydrogen bond between imidazole-NH and carbamate carbonyl.

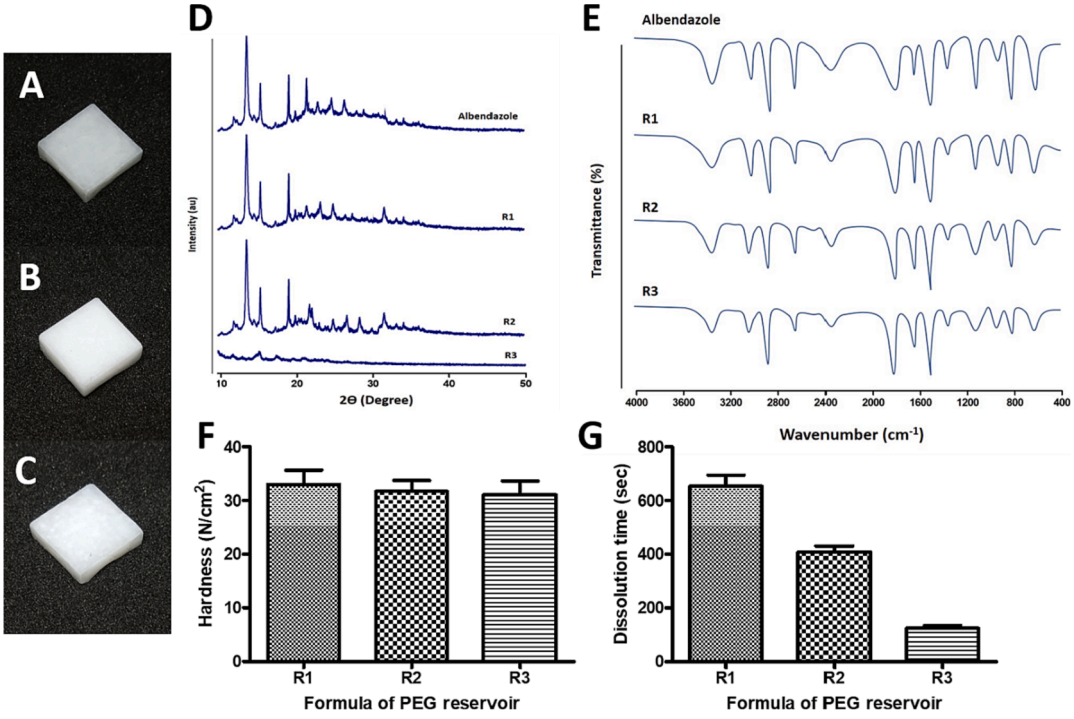

Fig. 5. The physical appearance of PEG reservoirs R1 (A), R2 (B), and R3 (C), respectively; the X-ray Diffractograms (D) and FTIR spectra (E) of pure ABZ and PEG reservoirs; hardness (F) and dissolution time (G) of PEG reservoir (mean ± SD, n = 3).

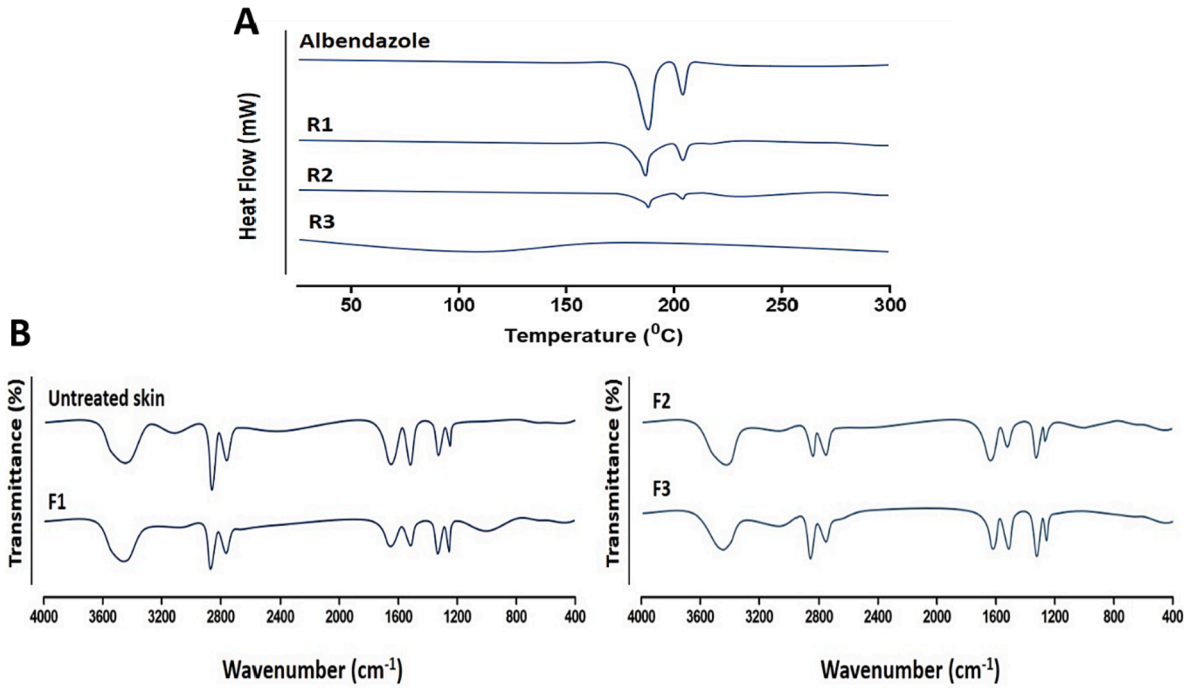

Fig. 6. Comparative DSC thermograms of albendazole and albendazole-PEG reservoirs (a); FTIR spectra of untreated skin and skin treated with HFM formulas (b).

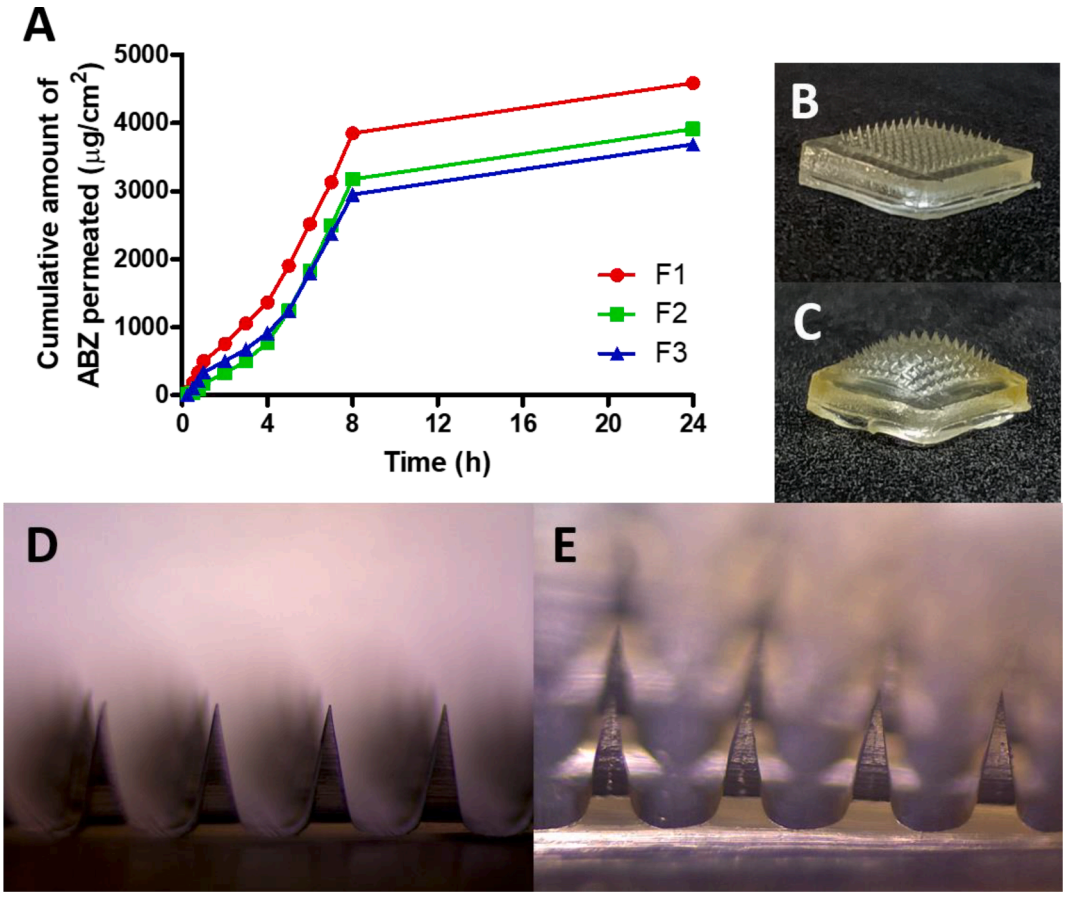

Fig. 7. Ex vivo permeation study of HFM integrated R3 (means + SD, n = 3) (A); macroscopic appearance of HFM before *ex vivo* (B) and after *ex vivo* (C); macroscopic comparison of HFM before *ex vivo* (D) and after *ex vivo* (E).

Importantly, all these IR spectra results showed that all the observed reservoirs have the same peaks as ABZ, which confirmed the presence of ABZ in the PEG reservoirs.

3.12. Ex vivo permeation study

The ex vivo permeation test is a study that is performed to determine the drug release profile from the MN after it has been applied to the skin. This assay describes the release of ABZ from a MN applied to the donor compartment to the receptor compartment via rat skin. Franz diffusion cells were used in the experiment, with sampling time intervals of 0.25, 0.5, 0.75, 1, 2, 3, 4, 5, 6, 7, 8, and 24 h. Permeated levels of ABZ were measured using a UV–Vis spectrophotometer at a wavelength of 298.2 nm. Based on the study in **Section 3.9**, R3 was selected to proceed to the *ex vivo* permeation study. The permeation profiles of the combination of HFM F1, F2, F3, with reservoir R3 are shown in Fig. 7**A**. After 24 h, ABZ permeated from HFM F1 was 4584.43 ± 26.61 μg/cm^2. The ABZ permeated from HFM F2 was 3911.07 ± 47.2 μg/cm^2. The ABZ permeated from HFM F3 was 3685.03 ± 44.91 μg/cm^2.

The percentage value of F1 permease is higher than other formulas, in accordance with the results of the swelling percentage test, which shows F1 has the highest swelling percentage compared to other formulas because of the shorter heating time. The swelling process describes an HFM that swells when it absorbs skin interstitial fluid, dissolves the drug in the reservoir, and delivers it through the stratum corneum [54]. The higher the swelling percentage, the more fluid is absorbed, and the faster the drug is released.

After statistical analysis, it was found that there was a significant difference ($p < 0.05$) between the combination of the three formulas of HFM with the R3 reservoir. Flux describes the amount of drug that can pass through an area at a particular time [55]. The flux values of all HFM integrated reservoir formulas had a significant difference ($p < 0.05$). Moreover, the permeation profile of all formulas shows biphasic release behaviour.

3.13. Skin integrity

After evaluation of skin integrity using FTIR (Fig. 6**B**), the untreated skin exhibited peaks at 2912 cm^{-1} as a result of asymmetric stretching of the hydrocarbons and 2803 cm^{-1} caused by symmetric CH_2 stretching. The presence of hydrocarbon areas indicates the presence of ceramides and fatty acids contained in the *stratum corneum*. Other peaks were found at 1693 cm^{-1} and 1512 cm^{-1} due to the presence of amide I and amide II bonds in corneocytes' keratin, respectively [26]. All these peaks were seen in all treated skin with little changes in intensity. As a result, the administration of HFM had no effect on the skin's integrity.

3.14. Hemolytic test

Hemolytic assay was performed to determine the potential toxicity of the formulation. All the formulations had not demonstrated any significant hemolysis (5 %) at any of the tested concentrations, which is also demonstrated by the serum or plasma after the clear and transparent treatments (Fig. 8). The hemolysis percentage values were close to the negative control, which was<5 %, based on the clear supernatant obtained after incubation with red blood cells. It is considered safe when the hemolysis index is<5 % [56]. The findings suggest that transdermal administration of ABZ and HFMs is likely to be safe.

Microneedle (MN) arrays use tens to hundreds of micron-sized needles, providing a painless option to increase skin permeability and enhance transdermal transmission. This microneedle array can be implemented in various applications, such as medical diagnosis, home diagnosis, beauty/clinic, medical treatment, and medical equipment [57]. Therefore, one thing that needs to be considered is the issue of HFM sterilization. MN research is a promising field of research to be pursued more extensively as it can be used to overcome the skin's natural defensive barrier, the stratum corneum, in both adults and children [58]. Several previous studies have shown that repeated application of MNs into the skin does not cause a decrease in skin barrier function. In addition, the use of polymer-based MNs, such as HFMN, has been shown not to stimulate the humoral immune system. The hydrogel-forming MN delivery system, which swells when it absorbs skin interstitial fluid, and stimulates drug permeation from the attached reservoir, makes this HFMN array biocompatible with good characterization. Therefore, considering the sterility of the device and biological load, further research is needed to become a convincing therapeutic safety record for hydrogel platforms [11]. In the production of microneedles, aseptic processes and gamma sterilization are feasible sterilization processes because the use of wet and humid heat can damage the device. According to previous study by McCrudden *et al.* (2015), when utilized properly, HFM integrated with a lyophilized wafer drug reservoir loaded with OVA and ibuprofen sodium poses a very low danger to human health, as shown by low endotoxin levels and the absence of microbial contamination. However, in order to avoid the expense and hassle of the aseptic process and if absolute sterility of MN products is finally required by the authorities, it is vital to explore the effect of lower gamma doses for the sterilizing process so as not to affect the drug load [59].

In terms of manufacturing and distribution challenge, the choice of material for the MN manufacturing and properties of kinetics for the drug release will play a pivotal role in the transformation of MNs into commercialized applications for effective treatments for various ailments. Material choices are hypercritical, and they should be capable of controlling the manner of drug release dynamics and their stability during manufacturing for the safe and effective usage of MNs [60]. In addition, there have been many clinical trials and technological advances for MNs that prove that MNs have the potential to be used

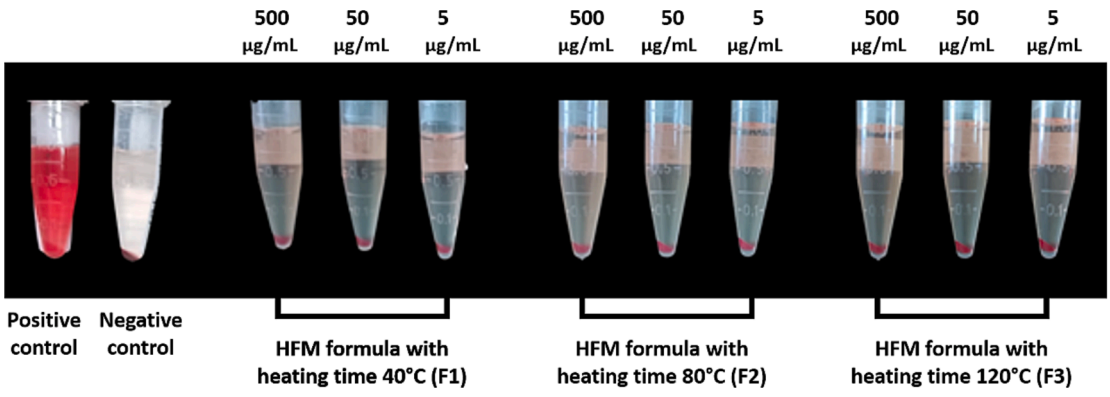

Fig. 8. Hemolytic assay of all the HFM integrated with PEG reservoirs.

commercially. Several MNs devices have been known to reach the commercial market for diagnostic and therapeutic applications [61].

Regarding the disposal of the microneedle, it has been studied previously that hydrogel-forming microneedles (HFM) helps reduce the needle waste as it forms a hydrogel matrix after application. Since MN arrays that generate hydrogels are self-disabling and cannot be reused, the disposal of the HFM is secure with low to none chance of infection transmission and accidental needle sticks injury [62]. In addition, the polymers and crosslinking agent used in this study are degradable [40]. The HFM matrix can be discarded as non-sharps waste, which is similar to a used bandage. Therefore, to some degree, the patient can just discard them in household waste without the need for a specialised waste container.

Finally, an innovative alternative treatment for cystic echinococcus was developed for the first time using HFM and PEG reservoir combination. The overall results showed that this dosage form has a higher potential for transdermal bioavailability and can deliver ABZ more quickly. Additionally, it has been shown that this combination of preparation is painless and non-irritating. However, this dosage form is still in the early phase of drug development. Therefore, further in vivo studies are needed to ascertain the plasma drug concentration and determine the required dosage.

4. Conclusion

The HFM that was integrated with the PEG reservoir has been successfully developed with PVA and PVP as polymers and citric acid as crosslinking agents. HFM has been evaluated through the swelling, mechanical, and insertion properties which showed that the matrix used can produce strong HFM and swell rapidly in the presence of interstitial fluid in the skin. The developed PEG reservoir has also been evaluated through hardness, dissolution time, as well as XRD and FTIR profiles, which showed that the reservoir has sufficient resistance for storage. The permeation test results through rats' skin also showed that the combination of these two dosage forms was safe, painless, and non-irritating. It also has a promising advantage in increasing ABZ bioavailability in the treatment of cystic echinococcosis.

CRediT authorship contribution statement

Ulfah Mahfufah: Conceptualization, Methodology, Funding acquisition, Writing – original draft. **Nurul Aisha Fitri Sultan:** Writing – original draft. **Andi Maqhfirah Nurul Fitri:** Writing – original draft. **Diany Elim:** Writing – original draft. **Muhammad Alif Sya'ban Mahfud:** Writing – original draft. **Nurfadilla Wafiah:** Methodology. **Rissa Ardita Friandini:** Methodology. **Lutfi Chabib:** Writing – review & editing. **Aliyah:** Supervision. **Andi Dian Permana:** Conceptualization, Project administration, Funding acquisition, Supervision.

Declaration of Competing Interest

The authors declare that they have no known competing financial interests or personal relationships that could have appeared to influence the work reported in this paper.

Data availability

No data was used for the research described in the article.

References

[1] A.D. Permana, A.J. Paredes, F. Volpe-Zanutto, Q.K. Anjani, E. Utomo, R. F. Donnelly, Dissolving microneedle-mediated dermal delivery of itraconazole nanocrystals for improved treatment of cutaneous candidiasis, Eur. J. Pharm. Biopharm. 154 (2020) 50–61, https://doi.org/10.1016/j.ejpb.2020.06.025.

[2] P. Deplazes, L. Rinaldi, C.A. Alvarez Rojas, P.R. Torgerson, M.F. Harandi, T. Romig, D. Antolova, J.M. Schurer, S. Lahmar, G. Cringoli, J. Magambo, R.C.A. Thompson, E.J. Jenkins, Global Distribution of Alveolar and Cystic Echinococcosis, Adv. Parasitol. 95 (2017) 315–493, https://doi.org/10.1016/bs.apar.2016.11.001.

[3] I.M. Dumitru, Medical Treatment of Cystic Echinococcosis, Overv. Echinococcosis. (2019), https://doi.org/10.5772/INTECHOPEN.88545.

[4] E. Brunetti, P. Kern, D.A. Vuitton, Expert consensus for the diagnosis and treatment of cystic and alveolar echinococcosis in humans, Acta Trop. 114 (2010) 1–16, https://doi.org/10.1016/j.actatropica.2009.11.001.

[5] A.D. Permana, A.J. Paredes, F.V. Zanutto, M.N. Amir, I. Ismail, M.A. Bahar, Sumarheni, S.D. Palma, R.F. Donnelly, Albendazole Nanocrystal-Based Dissolving Microneedles with Improved Pharmacokinetic Performance for Enhanced Treatment of Cystic Echinococcosis, ACS Appl. Mater. Interfaces. 13 (32) (2021) 38745–38760.

[6] S. Sawatdee, A. Atipairin, A. Sae Yoon, T. Srichana, N. Changsan, T. Suwandecha, Formulation development of albendazole-loaded self-microemulsifying chewable tablets to enhance dissolution and bioavailability, Pharmaceutics. 11 (3) (2019) 134.

[7] D. Ochoa, M. Saiz-Rodríguez, E. González-Rojano, S. Román, A. Sánchez-Rojas, A. Wojnicz, A. Ruiz-Nuño, F.-S. García-Arieta, High-Fat Breakfast Increases Bioavailability of Albendazole Compared to Low-Fat Breakfast: Single-Dose Study in Healthy Subjects, Front. Pharmacol. 13 (2021) 3875–38760.

[8] H. Cheng, M. Liu, X. Du, J. Xu, Y. Zhai, J. Ji, S. He, G. Zhai, Recent progress of micro-needle formulations: Fabrication strategies and delivery applications, J. Drug Deliv. Sci. Technol. 50 (2019) 18–26, https://doi.org/10.1016/j.jddst.2019.01.002.

[9] E. Larrañeta, R.E.M. Lutton, A.J. Brady, E.M. Vicente-Pérez, A.D. Woolfson, R.R. S. Thakur, R.F. Donnelly, Microwave-assisted preparation of hydrogel-forming microneedle arrays for transdermal drug delivery applications, Macromol. Mater. Eng. 300 (2015) 586–595, https://doi.org/10.1002/mame.201500016.

[10] R.F. Donnelly, M.T.C. McCrudden, A. Zaid Alkilani, E. Larrañeta, E. McAlister, A. J. Courtenay, M.-C. Kearney, T.R.R. Singh, H.O. McCarthy, V.L. Kett, E. Caffarel-Salvador, S. Al-Zahrani, A.D. Woolfson, M. Yamamoto, Hydrogel-forming microneedles prepared from "super swelling" polymers combined with lyophilised wafers for transdermal drug delivery, PLoS One. 9 (10) (2014) e111547.

[11] M.-C. Kearney, P.E. McKenna, H.L. Quinn, A.J. Courtenay, E. Larrañeta, R. F. Donnelly, Design and development of liquid drug reservoirs for microneedle delivery of poorly soluble drug molecules, Pharmaceutics. 11 (11) (2019) 605.

[12] L.K. Vora, K. Moffatt, I.A. Tekko, A.J. Paredes, F. Volpe-Zanutto, D. Mishra, K. e. Peng, R. Raj Singh Thakur, R.F. Donnelly, Microneedle array systems for long-acting drug delivery, Eur. J. Pharm. Biopharm. 159 (2021) 44–76.

[13] H. Van Ngo, V.T. Ngo, V.T. Vo, P.K. Nguyen, T.V. Van, P.H. Tran, T.T. Tran, Effects of absorbent on the dissolution rate of PEG-based solid dispersions containing poorly water-soluble drug, Springer Nat. (2018) 515–518.

[14] P.L. Pingale, A.P. Rajput, S.B. Bagade, Use of Natural Superdintegrants in Formulationof Fast Disintegrating Tablet of Atenolol, Eur. J. Mol. Clin. Med. 07 (2020) 3743–3752.

[15] R. He, Y. Niu, Z. Li, A. Li, H. Yang, F. Xu, F. Li, A Hydrogel Microneedle Patch for Point-of-Care Testing Based on Skin Interstitial Fluid, Adv. Healthc. Mater. 9 (2020) 1–11, https://doi.org/10.1002/adhm.201901201.

[16] I.A. Tekko, G. Chen, J. Domínguez-Robles, R.R.S. Thakur, I.M.N. Hamdan, L. Vora, E. Larrañeta, J.C. McElnay, H.O. McCarthy, M. Rooney, R.F. Donnelly, Development and characterisation of novel poly (vinyl alcohol)/poly (vinyl pyrrolidone)-based hydrogel-forming microneedle arrays for enhanced and sustained transdermal delivery of methotrexate, Int. J. Pharm. 586 (2020), 119580, https://doi.org/10.1016/j.ijpharm.2020.119580.

[17] A.D. Permana, M.T.C. McCrudden, R.F. Donnelly, Enhanced intradermal delivery of nanosuspensions of antifilariasis drugs using dissolving microneedles: A proof of concept study, Pharmaceutics. 11 (2019) 1–22, https://doi.org/10.3390/pharmaceutics11070346.

[18] Q.K. Anjani, A.D. Permana, Á. Cárcamo-Martínez, J. Domínguez-Robles, I. A. Tekko, E. Larrañeta, L.K. Vora, D. Ramadon, R.F. Donnelly, Versatility of hydrogel-forming microneedles in in vitro transdermal delivery of tuberculosis drugs, Eur. J. Pharm. Biopharm. 158 (2021) 294–312, https://doi.org/10.1016/j.ejpb.2020.12.003.

[19] T.R. Raj Singh, P.A. McCarron, A.D. Woolfson, R.F. Donnelly, Investigation of swelling and network parameters of poly(ethylene glycol)-crosslinked poly(methyl vinyl ether-co-maleic acid) hydrogels, Eur. Polym. J. 45 (2009) 1239–1249, https://doi.org/10.1016/j.eurpolymj.2008.12.019.

[20] E.A. Kamoun, E.R.S. Kenawy, T.M. Tamer, M.A. El-Meligy, M.S. Mohy Eldin, Poly (vinyl alcohol)-alginate physically crosslinked hydrogel membranes for wound dressing applications: Characterization and bio-evaluation, Arab. J. Chem. 8 (2015) 38–47, https://doi.org/10.1016/J.ARABJC.2013.12.003.

[21] P. González-Vázquez, E. Larrañeta, M.T.C. McCrudden, C. Jarrahian, A. Rein-Weston, M. Quintanar-Solares, D. Zehrung, H. McCarthy, A.J. Courtenay, R. F. Donnelly, Transdermal delivery of gentamicin using dissolving microneedle arrays for potential treatment of neonatal sepsis, J. Control. Release. 265 (2017) 30–40, https://doi.org/10.1016/j.jconrel.2017.07.032.

[22] P.W.R. Ananda, D. Elim, H.S. Zaman, W. Muslimin, M.G.R. Tunggeng, A. D. Permana, Combination of transdermal patches and solid microneedles for improved transdermal delivery of primaquine, Int. J. Pharm. 609 (2021), 121204, https://doi.org/10.1016/j.ijpharm.2021.121204.

[23] R.K. Basha, K. Konno, H. Kani, T. Kimura, Water vapor transmission rate of biomass based film materials, Eng. Agric. Environ. Food. 4 (2011) 37–42, https://doi.org/10.1016/S1881-8366(11)80018-2.

[24] L. Rahman, R.S. Lembang, S. Lallo, S.R. Handayani, Usmanengsi, A.D. Permana, Bioadhesive dermal patch as promising approach for improved antibacterial activity of bioactive compound of Zingiber cassumunar Roxb in ex vivo

Staphylococcus aureus skin infection model, J. Drug Deliv Sci. Technol. 63 (2021), 102522, https://doi.org/10.1016/j.jddst.2021.102522.
[25] K.R. Vandana, P.R. Yalavarthi, H.C. Vadlamudi, J.K.Y. Kalluri, A. Rasheed, Process, physicochemical characterization and in-vitro assessment of Albendazole microcrystals, Adv. Pharm. Bull. 7 (2017) 419–425, https://doi.org/10.15171/apb.2017.050.
[26] S. Talib, N. Ahmed, D. Khan, G.M. Khan, A. ur Rehman, Chitosan-chondroitin based artemether loaded nanoparticles for transdermal drug delivery system, J. Drug Deliv Sci. Technol. 61 (2021), 102281, https://doi.org/10.1016/j.jddst.2020.102281.
[27] M. Mir, A.D. Permana, I.A. Tekko, H.O. McCarthy, N. Ahmed, A.u. Rehman, R. F. Donnelly, Microneedle liquid injection system assisted delivery of infection responsive nanoparticles: A promising approach for enhanced site-specific delivery of carvacrol against polymicrobial biofilms-infected wounds, Int. J. Pharm. 587 (2020) 119643.
[28] M. Li, N. Qiao, K. Wang, Influence of Sodium Lauryl Sulfate and Tween 80 on Carbamazepine-Nicotinamide Cocrystal Solubility and Dissolution Behaviour, Pharmaceutics. 5 (2013) 508–524, https://doi.org/10.3390/pharmaceutics5040508.
[29] J. Ramyasree, A.A. Hindustan, H. Chinthaguinjala, T. Reshma, H.V. Chenga Venkata, K., Yedire Bharath, Solubility Enhancement of Drugs with Aid of Surfactants: Research Done Since Last Two Decades, Int. J. Pharma Bio Sci. 10 (2020), https://doi.org/10.22376/IJPBS/LPR.2020.10.5.P11-16.
[30] M.A. El-Massik, I.A. Darwish, E.E. Hassan, L.K. El-Khordagui, Development of a dissolution medium for glibenclamide, Int. J. Pharm. 140 (1996) 69–76, https://doi.org/10.1016/0378-5173(96)04580-2.
[31] T. Taupitz, S. Klein, Can biorelevant media be simplified by using SLS and Tween 80 to replace bile compounds? Open Drug Deliv. J. 4 (2010) 30–37, https://doi.org/10.2174/1874126601004020030.
[32] T. Waghule, G. Singhvi, S.K. Dubey, M.M. Pandey, G. Gupta, M. Singh, K. Dua, Microneedles: A smart approach and increasing potential for transdermal drug delivery system, Biomed. Pharmacother. 109 (2019) 1249–1258, https://doi.org/10.1016/j.biopha.2018.10.078.
[33] L. Yu, L. Gu, Hydrolyzed polyacrylonitrile-blend-soy protein hydrogel fibers: A study of structure and dynamic pH response, Polym. Int. 58 (2009) 66–73, https://doi.org/10.1002/pi.2493.
[34] T. Tan, J. Zhou, X. Gao, X. Tang, H. Zhang, Synthesis, characterization and water-absorption behavior of tartaric acid-modified cellulose gel fromcorn stalk pith, Ind. Crops Prod. 169 (2021), 113641, https://doi.org/10.1016/j.indcrop.2021.113641.
[35] A.D. Permana, Q.K. Anjani, Sartini, E. Utomo, F. Volpe-Zanutto, A.J. Paredes, Y. M. Evary, S.A. Mardikasari, M.R. Pratama, I.N. Tuany, R.F. Donnelly, Selective delivery of silver nanoparticles for improved treatment of biofilm skin infection using bacteria-responsive microparticles loaded into dissolving microneedles, Mater. Sci. Eng. 120 (2021) 111786.
[36] A.K. Sonker, V. Verma, Influence of crosslinking methods toward poly(vinyl alcohol) properties: Microwave irradiation and conventional heating, J. Appl. Polym. Sci. 135 (2018) 46125, https://doi.org/10.1002/APP.46125.
[37] A.Z. Alkilani, M.T.C. McCrudden, R.F. Donnelly, Transdermal drug delivery: Innovative pharmaceutical developments based on disruption of the barrier properties of the stratum corneum, Pharmaceutics. 7 (2015) 438–470, https://doi.org/10.3390/pharmaceutics7040438.
[38] X.P. Zhang, B.B. Wang, W.X. Li, W.M. Fei, Y. Cui, X.D. Guo, In vivo safety assessment, biodistribution and toxicology of polyvinyl alcohol microneedles with 160-day uninterruptedly applications in mice, Eur. J. Pharm. Biopharm. 160 (2021) 1–8, https://doi.org/10.1016/J.EJPB.2021.01.005.
[39] L. Kagan, P. Gershkovich, A. Mendelman, S. Amsili, N. Ezov, A. Hoffman, The role of the lymphatic system in subcutaneous absorption of macromolecules in the rat model, Eur. J. Pharm. Biopharm. 67 (2007) 759–765, https://doi.org/10.1016/J.EJPB.2007.04.002.
[40] S. Thongsuksaengcharoen, S. Samosorn, K. Songsrirote, A Facile Synthesis of Self-Catalytic Hydrogel Films and Their Application as a Wound Dressing Material Coupled with Natural Active Compounds, ACS Omega. 5 (2020) 25973–25983, https://doi.org/10.1021/acsomega.0c03414.
[41] H.M. Zidan, E.M. Abdelrazek, A.M. Abdelghany, A.E. Tarabiah, Characterization and some physical studies of PVA/PVP filled with MWCNTs, J. Mater. Res. Technol. 8 (2019) 904–913, https://doi.org/10.1016/j.jmrt.2018.04.023.
[42] E. Larrañeta, J. Moore, E.M. Vicente-Pérez, P. González-Vázquez, R. Lutton, A. D. Woolfson, R.F. Donnelly, A proposed model membrane and test method for microneedle insertion studies, Int. J. Pharm. 472 (2014) 65–73, https://doi.org/10.1016/J.IJPHARM.2014.05.042.
[43] E.M. Vicente-Pérez, H.L. Quinn, E. McAlister, S. O'Neill, L.A. Hanna, J.G. Barry, R. F. Donnelly, The Use of a Pressure-Indicating Sensor Film to Provide Feedback upon Hydrogel-Forming Microneedle Array Self-Application In Vivo, Pharm. Res. 33 (2016) 3072–3080, https://doi.org/10.1007/S11095-016-2032-Z/FIGURES/3.
[44] R.F. Donnelly, K. Moffatt, A.Z. Alkilani, E.M. Vicente-Pérez, J. Barry, M.T. C. McCrudden, A.D. Woolfson, Hydrogel-forming microneedle arrays can be effectively inserted in skin by self-application: a pilot study centred on pharmacist intervention and a patient information leaflet, Pharm. Res. 31 (2014) 1989–1999, https://doi.org/10.1007/S11095-014-1301-Y.
[45] M.L. Cacicedo, G. Pacheco, G.A. Islan, V.A. Alvarez, H.S. Barud, G.R. Castro, Chitosan-bacterial cellulose patch of ciprofloxacin for wound dressing: Preparation and characterization studies, Int. J. Biol. Macromol. 147 (2020) 1136–1145, https://doi.org/10.1016/J.IJBIOMAC.2019.10.082.
[46] V. Michailova, S. Titeva, R. Kotsilkova, E. Krusteva, E. Minkov, Water uptake and relaxation processes in mixed unlimited swelling hydrogels, Int. J. Pharm. 209 (2000) 45–56, https://doi.org/10.1016/S0378-5173(00)00536-6.
[47] B.K. Abdul Rasool, A.A. Mohammed, Y.Y. Salem, The optimization of a dimenhydrinate transdermal patch formulation based on the quantitative analysis of in vitro release data by DDSolver through skin penetration studies, Sci. Pharm. 89 (3) (2021) 33.
[48] T. Mehrotra, M.N. Zaman, B.B. Prasad, A. Shukla, S. Aggarwal, R. Singh, Rapid immobilization of viable Bacillus pseudomycoides in polyvinyl alcohol/glutaraldehyde hydrogel for biological treatment of municipal wastewater, Environ. Sci. Pollut. Res. Int. 27 (2020) 9167–9180, https://doi.org/10.1007/S11356-019-07296-Z.
[49] S. Afifi, Solid Dispersion Approach Improving Dissolution Rate of Stiripentol: a Novel Antiepileptic Drug, Shaheed Beheshti Univ, Med. Sci. Heal. Serv. Iran. J. Pharm. Res. 14 (2015) 1001–1014.
[50] P.P. Lestari, E. Budianto, Controlled Drug Delivery Carrier of Nifedipine Using Biodegradable Microcapsule Polymer from Poly (D, L-Lactic Acid) and Polyethylene Glycol, J. Phys. Conf. Ser. 1751 (1) (2021) 012082.
[51] K.D. Koradia, R.H. Parikh, H.D. Koradia, Albendazole nanocrystals: Optimization, spectroscopic, thermal and anthelmintic studies, J. Drug Deliv. Sci. Technol. 43 (2018) 369–378, https://doi.org/10.1016/j.jddst.2017.11.003.
[52] F.K. Alanazi, M. El-Badry, M.O. Ahmed, I.A. Alsarra, Improvement of Albendazole Dissolution by Preparing Microparticles Using Spray-Drying Technique, n.d.
[53] D.H. Won, M.S. Kim, S. Lee, J.S. Park, S.J. Hwang, Improved physicochemical characteristics of felodipine solid dispersion particles by supercritical anti-solvent precipitation process, Int. J. Pharm. 301 (2005) 199–208, https://doi.org/10.1016/J.IJPHARM.2005.05.017.
[54] R.F. Donnelly, R. Majithiya, T.R.R. Singh, D.I.J. Morrow, M.J. Garland, Y.K. Demir, K. Migalska, E. Ryan, D. Gillen, C.J. Scott, A.D. Woolfson, Design, optimization and characterisation of polymeric microneedle arrays prepared by a novel laser-based micromoulding technique, Pharm. Res. 28 (2011) 41–57, https://doi.org/10.1007/s11095-010-0169-8.
[55] M. Silva-Abreu, L. Espinoza, L. Halbaut, M. Espina, M. García, A. Calpena, Comparative Study of Ex Vivo Transmucosal Permeation of Pioglitazone Nanoparticles for the Treatment of Alzheimer's Disease, Polymers (Basel). 10 (3) (2018) 316.
[56] H.Y. Zhou, Y.P. Zhang, W.F. Zhang, X.G. Chen, Biocompatibility and characteristics of injectable chitosan-based thermosensitive hydrogel for drug delivery, Carbohydr. Polym. 83 (2011) 1643–1651, https://doi.org/10.1016/j.carbpol.2010.10.022.
[57] N.G. Oh, S.Y. Hwang, Y.H. Na, Fabrication of a PVA-Based Hydrogel Microneedle Patch, ACS Omega. 7 (2022) 25179–25185, https://doi.org/10.1021/acsomega.2c01993.
[58] K. Cheung, D.B. Das, Microneedles for drug delivery: trends and progress, Drug Deliv. 23 (2016) 2338–2354, https://doi.org/10.3109/10717544.2014.986309.
[59] M.T.C. McCrudden, A.Z. Alkilani, A.J. Courtenay, C.M. McCrudden, B. McCloskey, C. Walker, N. Alshraiedeh, R.E.M. Lutton, B.F. Gilmore, A.D. Woolfson, R. F. Donnelly, Considerations in the sterile manufacture of polymeric microneedle arrays, Drug Deliv, Transl. Res. 5 (2015) 3–14, https://doi.org/10.1007/s13346-014-0211-1.
[60] A.K. Gera, R.K. Burra, The Rise of Polymeric Microneedles: Recent Developments, Advances, Challenges, and Applications with Regard to Transdermal Drug Delivery, J. Funct. Biomater. 13 (2) (2022) 81.
[61] N.G. Rouphael, M. Paine, R. Mosley, S. Henry, D.V. McAllister, H. Kalluri, W. Pewin, P.M. Frew, T. Yu, N.J. Thornburg, S. Kabbani, L. Lai, E.V. Vassilieva, I. Skountzou, R.W. Compans, M.J. Mulligan, M.R. Prausnitz, A. Beck, S. Edupuganti, S. Heeke, C. Kelley, W. Nesheim, The safety, immunogenicity, and acceptability of inactivated influenza vaccine delivered by microneedle patch (TIV-MNP 2015): a randomised, partly blinded, placebo-controlled, phase 1 trial, Lancet. 390 (2017) 649–658, https://doi.org/10.1016/S0140-6736(17)30575-5.
[62] E. Larrañeta, R.E.M. Lutton, A.D. Woolfson, R.F. Donnelly, Microneedle arrays as transdermal and intradermal drug delivery systems: Materials science, manufacture and commercial development, Mater. Sci. Eng. R Reports. 104 (2016) 1–32, https://doi.org/10.1016/j.mser.2016.03.001.